

Spectroscopic study of oxygen and fluorine isotopes with the $(\alpha, {}^3\text{He})$ and (α, t) reactions on ${}^{16,17,18}\text{O}$

M. Yasue,⁽¹⁾ T. Hasegawa,⁽²⁾ S. I. Hayakawa,⁽³⁾ K. Ieki,⁽⁴⁾ J. Kasagi,⁽⁵⁾ S. Kubono,⁽⁶⁾
T. Murakami,⁽⁷⁾ K. Nisimura,⁽⁸⁾ K. Ogawa,⁽⁹⁾ H. Ohnuma,⁽¹⁰⁾ R. J. Peterson,⁽¹¹⁾ H. Shimizu,⁽¹²⁾
M. H. Tanaka,⁽⁶⁾ and H. Toyokawa⁽¹³⁾

⁽¹⁾Miyagi University of Education, Sendai 980, Japan

⁽²⁾Faculty of Engineering, Miyazaki University, Miyazaki 889-21, Japan

⁽³⁾Ashikaga Institute of Technology, Ashikaga 326, Japan

⁽⁴⁾Department of Physics, Rikkyo University, Toshima, Tokyo 171, Japan

⁽⁵⁾Laboratory of Nuclear Science, Tohoku University, Sendai 982, Japan

⁽⁶⁾Institute for Nuclear Study, University of Tokyo, Tanashi, Tokyo 188, Japan

⁽⁷⁾Department of Physics, Kyoto University, Kyoto 606, Japan

⁽⁸⁾Tohoku Gakuin University, Izumi-ku, Sendai 981-31, Japan

⁽⁹⁾College of Arts and Science, Chiba University, Chiba 260, Japan

⁽¹⁰⁾Department of Physics, Tokyo Institute of Technology, Meguro, Tokyo 152, Japan

⁽¹¹⁾Nuclear Physics Laboratory, University of Colorado, Boulder, Colorado 80309

⁽¹²⁾Faculty of General Education, Yamagata University, Yamagata 990, Japan

⁽¹³⁾Tandem Accelerator Center, The University of Tsukuba, Ibaraki 305, Japan

(Received 15 June 1992)

The $(\alpha, {}^3\text{He})$ and (α, t) reactions on ${}^{16,17,18}\text{O}$ were studied at $E_\alpha = 65$ MeV. Measured cross sections for the states up to 15 MeV in the residual nuclei were analyzed with the distorted wave Born approximation theory. Many spin-parity and isospin assignments were proposed based on the strengths, angular distributions, and excitation energies. Nearly equal spectroscopic factors were obtained for bound and unbound analog pairs except for the 2_1^+ , $T=1$ states in ${}^{18}\text{O}$ and ${}^{18}\text{F}$. Almost full strengths were observed for the $0d_{5/2}$, $1s_{1/2}$, and $0d_{3/2}$ transfers. The obtained spectroscopic factors for the $0d_{5/2}$ and $1s_{1/2}$ transfers were in good agreement with shell-model calculations, while the agreement was unsatisfactory for the $0d_{3/2}$ transfer in many respects. The $d_{3/2}$ strengths in ${}^{17}\text{O}$ and ${}^{17}\text{F}$ were more fragmented than the shell-model prediction, while only half of the expected $0d_{3/2}$ strength was found in ${}^{18}\text{O}$ and ${}^{19}\text{O}$. The strength to the first excited $\frac{3}{2}^+$, $T=\frac{1}{2}$ state in ${}^{19}\text{F}$ was twice that predicted. Spectroscopic factors for many of $0f_{7/2}$ transitions were also deduced. The 14.1 and 14.3 MeV states in ${}^{18}\text{O}$, in particular, proposed to be the stretched 6^- states in a recent (e, e') experiment, were found to be excited by pure $l=3$ transfer with spectroscopic factors 0.16 and 0.05, respectively.

PACS number(s): 25.55.Hp, 27.20.+n

I. INTRODUCTION

Recent shell-model calculations for sd -shell nuclei [1] very well describe not only the level schemes but also dynamical properties, such as $E2$ transition probabilities [2] and spectroscopic factors [3]. However, unsatisfactory agreement between the experimental and theoretical spectroscopic factors for $0d_{3/2}$ transfer was noticed in a previous study [3] on $A=26$ nuclei. Problems are also reported for the matrix elements related to the $0d_{3/2}$ shell orbit. Jiang *et al.* [4] derived an sd -shell effective interaction from the Bonn NN potential, and found its matrix elements in overall good agreement with the empirical matrix elements of Wildenthal [1] except for those involving the $0d_{3/2}$ orbit. The shell-model calculations [1] for early sd -shell nuclei are based on an assumption of an ${}^{16}\text{O}$ inert core with $0d_{3/2}$ orbit lying about 5 MeV above the $0d_{5/2}$ and $1s_{1/2}$ orbits. A comparison of experimental and theoretical spectroscopic factors for the $0d_{3/2}$ transfer near ${}^{16}\text{O}$ therefore requires information on high-lying states, but previous single-nucleon transfer studies

on early sd -shell nuclei were restricted to low-lying states [5].

Recent observation of stretched states and $M1$ states in proton and electron inelastic scattering on early sd -shell nuclei promoted further interest in looking at high-lying states. A 1^+ state was found in ${}^{18}\text{O}$ at 8.82 MeV in proton scattering [6]. The shell-model calculation predicts a lowest 1^+ state in ${}^{18}\text{O}$ at 10.8 MeV which should be several times stronger in (p, p') than was observed. Additional information on such 1^+ states is clearly needed for the discussion of missing $M1$ strengths. A recent electron scattering experiment [7] on ${}^{18}\text{O}$ has located candidates for the 6^- states with the $(d_{5/2}, f_{7/2})$ structure at 14.1 and 14.3 MeV. Spectroscopic factors for these states, together with those for the $f_{7/2}$ single-particle strengths in $A=17$ and 19 nuclei, should give quantitative information on the fragmentation of such stretched states.

We have studied the $(\alpha, {}^3\text{He})$ and (α, t) reactions on ${}^{16}\text{O}$, ${}^{17}\text{O}$, and ${}^{18}\text{O}$ around $E_\alpha = 65$ MeV, and compared the obtained spectroscopic factors with shell-model predictions. The present measurements cover wide ranges of

excitation energies ($E_x < 10$ MeV for $A = 17$, $E_x < 15$ MeV for $A = 18$, and $E_x < 14$ MeV for $A = 19$) in order to obtain information on the $0d_{3/2}$ and $0f_{7/2}$ transfers. Measurements of both the $(\alpha, ^3\text{He})$ and (α, t) reactions under identical experimental conditions allow us direct comparisons of the neutron and proton strengths in the analog states.

II. EXPERIMENTAL PROCEDURE

Measurements were carried out with α beams from the sector-focusing cyclotron at the Institute for Nuclear

Study of the University of Tokyo. Incident energies were 64.9 MeV for ^{16}O and 64.3 MeV for ^{17}O and ^{18}O . Reaction products were analyzed by a magnetic spectrometer [8] and detected with a drift-type single wire proportional counter [9] backed up by two ΔE counters and an E counter. Self-supporting tantalum foil oxidized to Ta_2O_5 in the atmosphere of natural oxygen gas or of 98.7% enriched ^{18}O gas was used as a target. The oxygen content was measured to be 0.32 mg/cm² in the ^{16}O target and 0.25 mg/cm² in the ^{18}O target by comparing the yields of elastically scattered α particles with previous data [10].

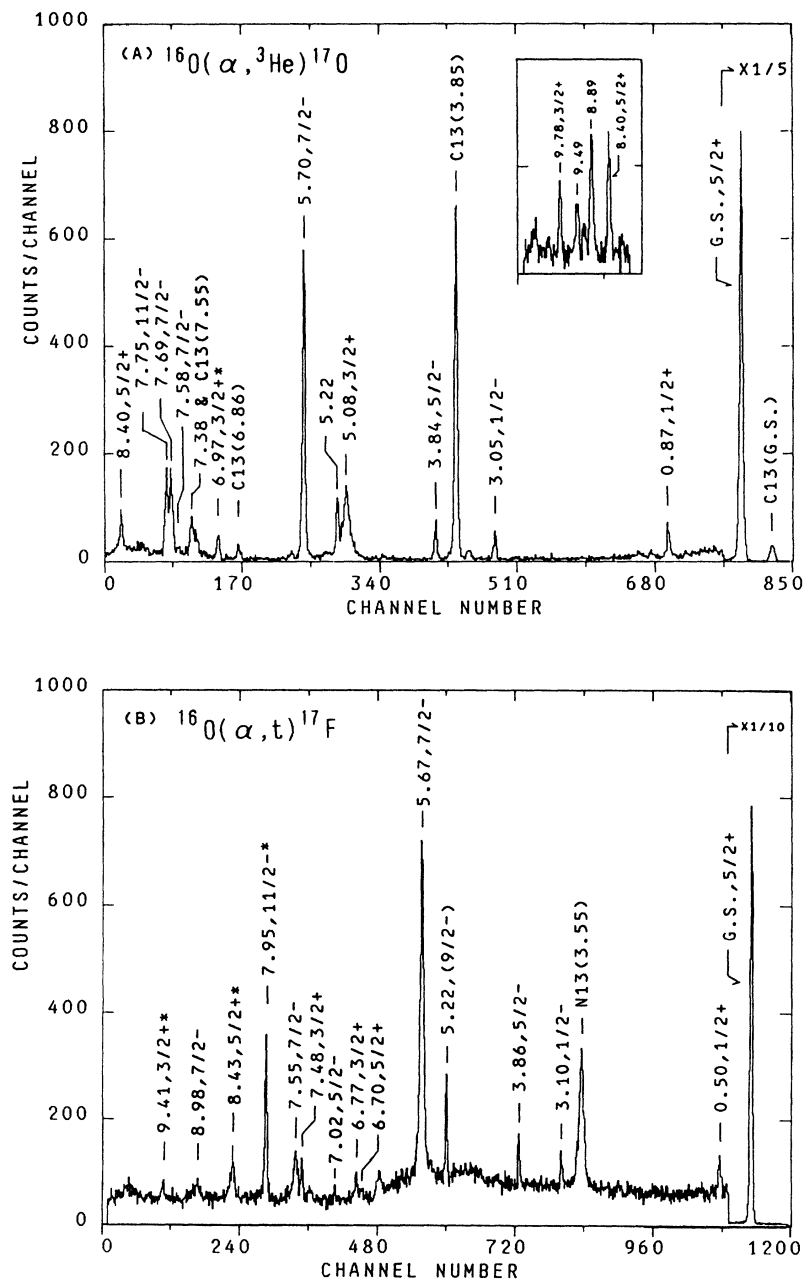


FIG. 1. Momentum spectra obtained at $E_\alpha = 64.9$ MeV and $\theta_{\text{lab}} = 10^\circ$ for (a) the $^{16}\text{O}(\alpha, ^3\text{He})^{17}\text{O}$ and (b) the $^{16}\text{O}(\alpha, t)^{17}\text{F}$ reactions. The inset in (a) shows a partial spectrum around $E_x = 8$ –10 MeV. Energy resolution for these spectra is 40 keV FWHM. The J^π values with an asterisk are those proposed in the present work.

A gas target cell [10] was used for ^{17}O , with 51.2% enriched $^{17}\text{O}_2$ gas at a pressure of 0.5 atm. Further details of the experiment are described in Ref. [10].

Typical momentum spectra are displayed in Figs. 1–3. The 5.0 MeV $\frac{3}{2}^+$ state in ^{17}F and the 5.33 MeV $\frac{3}{2}^+$ state in ^{19}O are known to have widths of 1.5 and 0.3 MeV, respectively [5]. Peaks corresponding to these states are too broad to be noticed in the spectra of Figs. 1 and 2, but appear clearly in packed spectra. Overall ambiguity in absolute values of cross sections for these broad states is about 30%, and that for other narrow states is about 15%. Relative errors in the cross sections are much

smaller. Obtained cross sections are shown in Figs. 4 through 15, where error bars include statistical errors and errors in the peak analyses and background subtraction.

III. DWBA ANALYSES

Cross sections for the $(\alpha, ^3\text{He})$ and (α, t) reactions were analyzed with the exact-finite-range (EFR) DWBA code TWOFNR [11]. The calculated cross sections σ_{TWO} are related to the experimental value σ_{exp} by $\sigma_{\text{exp}} = C^2 s S \sigma_{\text{TWO}}$, where S is a spectroscopic factor, s ($=2$) is the light parti-

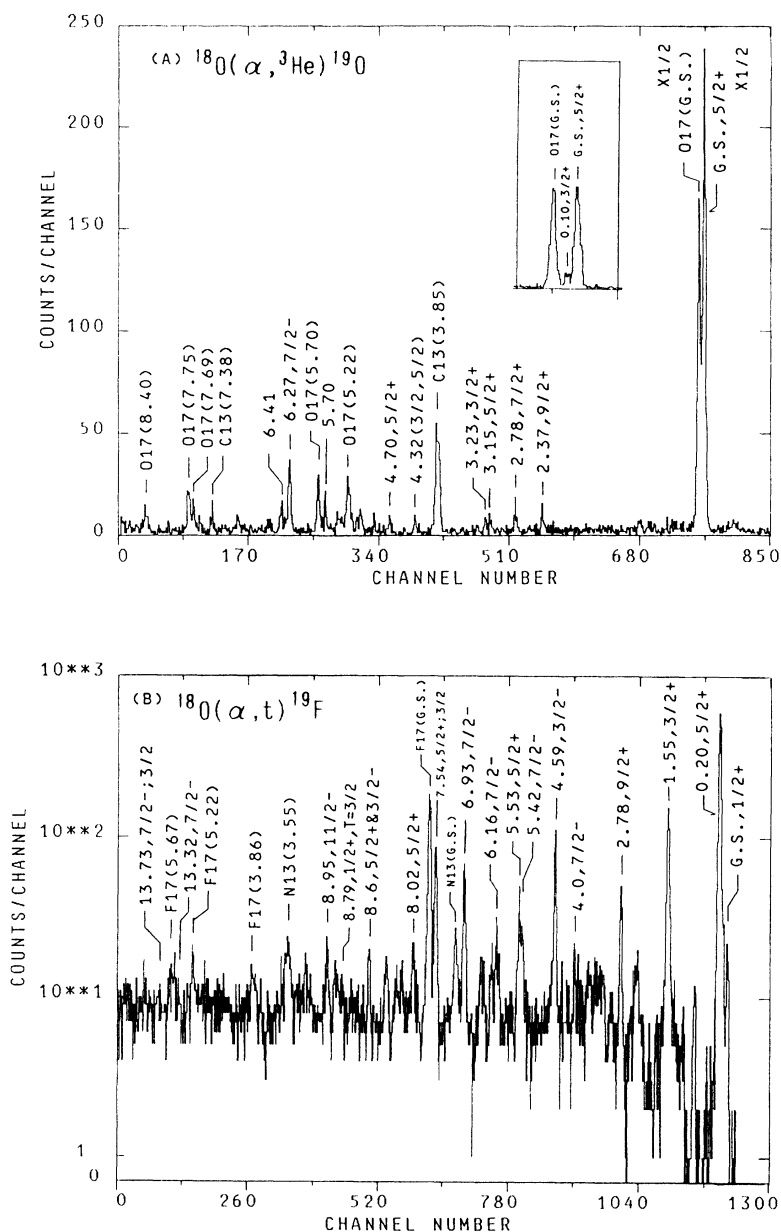


FIG. 2. Momentum spectra obtained at $E_\alpha = 64.3$ MeV and $\theta_{\text{lab}} = 20^\circ$ for (a) the $^{18}\text{O}(\alpha, ^3\text{He})^{19}\text{O}$ and (b) the $^{18}\text{O}(\alpha, t)^{19}\text{F}$ reactions. The inset in (a) shows a partial spectrum near the ground state at $\theta_{\text{lab}} = 30^\circ$. Energy resolutions for the spectra (a) and (b) are 30 and 50 keV FWHM, respectively.

cle spectroscopic factor, and C^2 is an isospin Clebsch-Gordan coefficient. Several transferred j values can be mixed in the stripping reaction on ^{17}O . Since we cannot distinguish experimentally $0d_{5/2}$ and $0d_{3/2}$ transfers to the states in ^{18}O and ^{18}F , DWBA cross sections weighted by the shell-model spectroscopic factors and summed over the transferred j are compared with the experimental cross sections. We used the zero-range (ZR) DWBA code DWUCK4 [12] with resonance form factors to calculate cross sections for unbound states. A finite range parameter of 0.7 fm and a nonlocality parameter of 0.2 fm

were used in the local energy approximation of ZR DWBA calculations [12]. The D_0^2 values for ZR calculations were determined by comparing the cross sections calculated by TWOFNR and DWUCK4 for bound states. They were $8.2 \times 10^4 \text{ MeV}^2 \text{ fm}^3$ for the $(\alpha, ^3\text{He})$ reaction, and $8.4 \times 10^4 \text{ MeV}^2 \text{ fm}^3$ for the (α, t) reaction. It was found that the calculated cross sections did not change smoothly with excitation energies for the states unbound by more than 4 MeV for $l=2$ transfer and more than 7 MeV for $l=3$ transfer. Hence we fixed the energies above the threshold to be 4 and 7 MeV for $l=2$ and 3

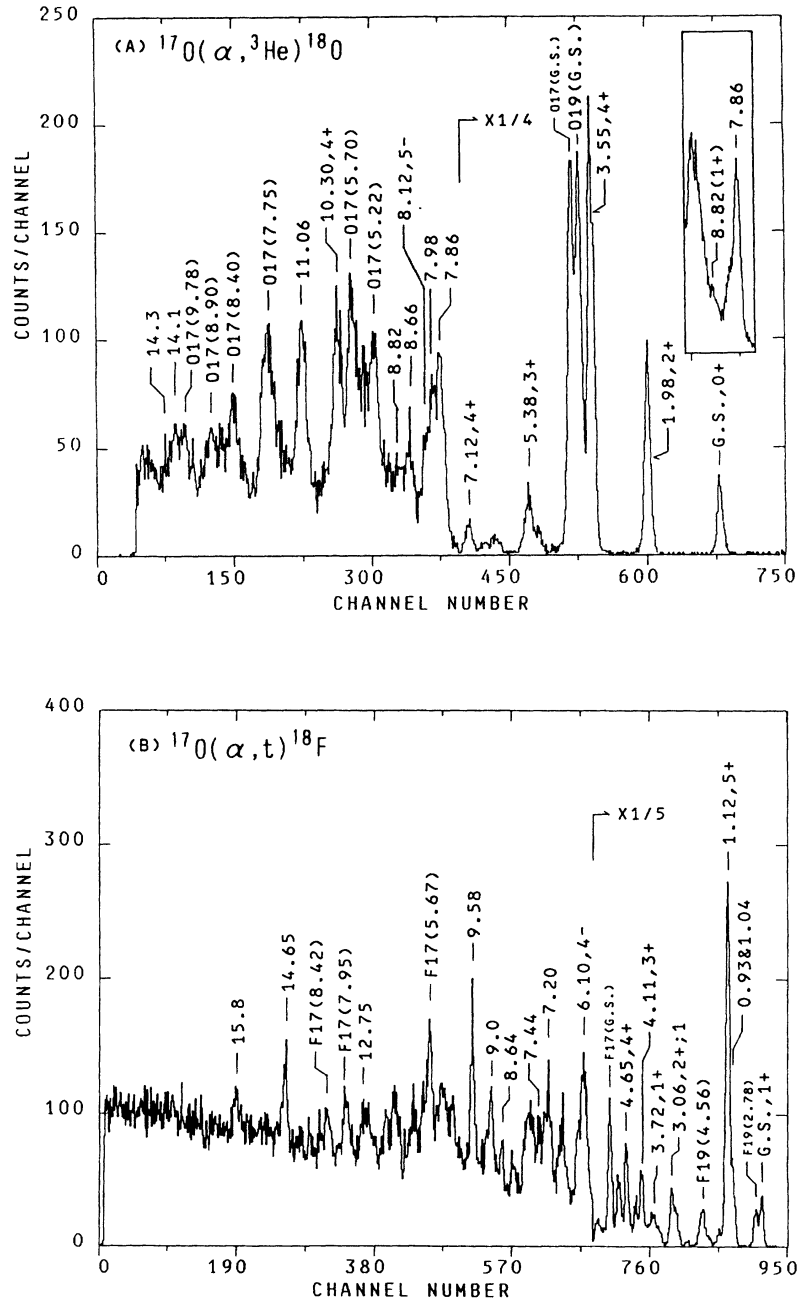


FIG. 3. Momentum spectra obtained at $E_\alpha = 64.3 \text{ MeV}$ and $\theta_{\text{lab}} = 30^\circ$ for (a) the $^{17}\text{O}(\alpha, ^3\text{He})^{18}\text{O}$ and (b) the $^{17}\text{O}(\alpha, t)^{18}\text{F}$ reactions. The inset in (a) shows a partial spectrum at $\theta_{\text{lab}} = 20^\circ$. Energy resolutions for the spectra (a) and (b) are 170 and 150 keV FWHM, respectively.

TABLE I. Potential parameters used in the present DWBA analyses.

Potential set	V_R (MeV)	r_R (fm)	a_R (fm)	W_V (MeV)	W_S (MeV)	r_W (fm)	a_W (fm)	V_{ls} (MeV)	r_C (fm)	$J_R/A1A2$ (MeV fm ³)
A0 ^a	205.9	1.47	0.556	34.7	0	1.35	0.49	0	1.4	837
A1 ^b	200	1.19	0.706	21	0	1.44	0.649	0	1.4	546
H1 ^c	145.1	1.38	0.631	0	18.73	1.40	0.631	4.53	1.25	702
HB ^d	149	1.20	0.72	29.4	0	1.4	0.88	2.5	1.3	553
Bound states		1.25	0.65					6.0	1.25	

^aReference [10].

^bParameters fitted to the data in Ref. [10].

^cReference [13].

^dReference [14].

transfers, respectively, for higher excited states.

Potential parameters used in the DWBA calculations were obtained from Refs. 10, 13, and 14, and listed in Table I. The parameter set A0 was used for α , and the set H1 for ^3He and t in the EFR DWBA calculations. In the ZR DWBA calculations, the parameter sets A1 and HB were used for the incoming and outgoing channels, respectively. The volume integrals of the real part of the A1 and HB potentials are similar to each other. Such a similarity was preferred for the ZR DWBA calculations. The EFR calculations with the parameter sets A0 and H1 gave better fit to angular distribution shapes for the $\frac{5}{2}^+$ and $\frac{1}{2}^+$ states of ^{17}O than those with the sets A1-HB. Thus different sets of potential parameters were used for the EFR and ZR calculations in the present analyses.

IV. RESULTS AND DISCUSSION

Measured angular distributions are displayed in Figs. 4–15 together with DWBA calculations. Deduced spectroscopic factors are listed in Tables II–IV, and compared with the shell-model predictions [1] and with the results of previous experiments [15–20]. Here we present only the data relevant to the direct transfer to the $0d_{5/2}$, $1s_{1/2}$, $0d_{3/2}$, and $0f_{7/2}$ shell orbits.

A. $(\alpha, ^3\text{He})$ and (α, t) reactions on ^{16}O with $l=2$ transfer

The cross sections for the $^{16}\text{O}(\alpha, ^3\text{He})^{17}\text{O}$ reaction leading to the $\frac{5}{2}^+$ and $\frac{3}{2}^+$ states are displayed in Fig. 4, where the solid and dashed curves show EFR and ZR DWBA calculations, respectively. Those for the $^{16}\text{O}(\alpha, t)^{17}\text{F}$ reaction are shown in Fig. 5. The angular distributions for the $\frac{5}{2}^+$ ground states in ^{17}O and ^{17}F are well reproduced at forward angles. Obtained spectroscopic factors for these states are considerably larger than unity (Table II), while the calculations with the parameter sets A1-HB give C^2S of 1.0 for the $\frac{5}{2}^+$ states of ^{17}O and ^{17}F with poorer fits to the angular distributions.

Two more $\frac{5}{2}^+$ states at 7.379 and 8.402 MeV are known [5] in ^{17}O . The 7.379 MeV state lies close to the 7.382 MeV $\frac{5}{2}^-$ state. A peak is seen at $E_x = 7.38$ MeV in the present spectra [Fig. 1(a)], but this was a contaminant peak due to the 7.55 MeV ($\frac{5}{2}^-$) state in ^{13}C . The corresponding 6.70 MeV $\frac{5}{2}^+$ and 7.02 MeV $\frac{5}{2}^-$ states in the

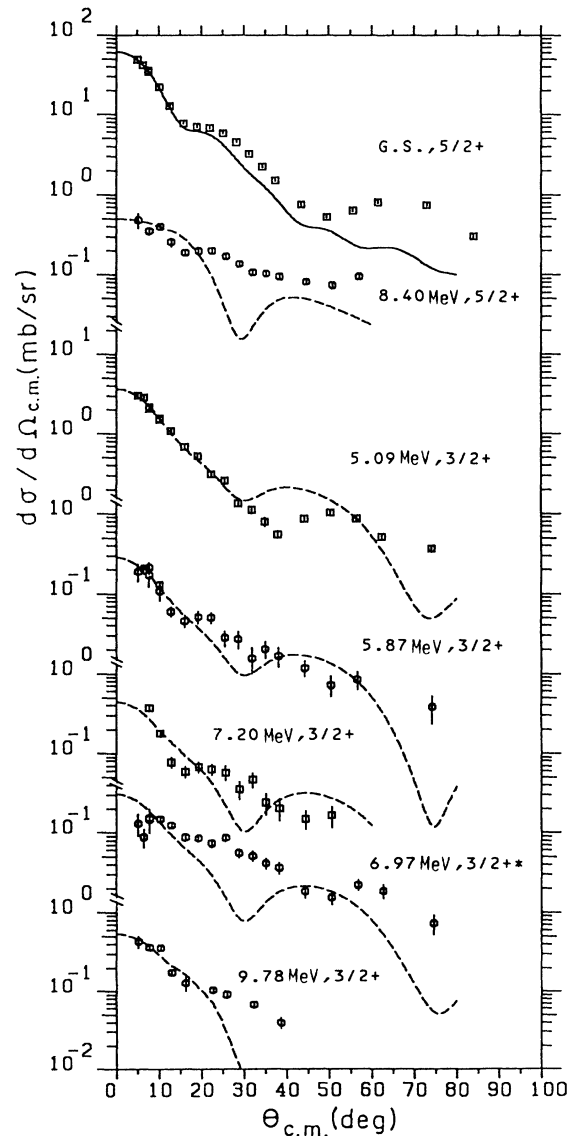


FIG. 4. Cross sections for the $^{16}\text{O}(\alpha, ^3\text{He})$ reaction leading to the $\frac{5}{2}^+$ and $\frac{3}{2}^+$ states in ^{17}O . The curves are EFR (solid) and ZR (dashed) DWBA calculations for the bound and unbound states, respectively. The J^π value with an asterisk is that proposed in the present work.

mirror nucleus ^{17}F were both very weakly excited. The (α, t) yields for the 6.70 MeV $\frac{5}{2}^+$ state of ^{17}F are only 0.2% of those for the $\frac{5}{2}^+$ ground state. On the other hand, the third $\frac{5}{2}^+$ state of ^{17}O at 8.40 MeV is clearly seen in Fig. 1(a), and has $(\alpha, ^3\text{He})$ yields about 1% of those for the $\frac{5}{2}^+$ ground state at forward angles. Its angular distribution is somewhat different from that for the ground state, and does not show a steep rise at small angles. Our DWBA calculation reproduces overall the slope of the measured angular distribution, although it shows a minimum around 30° which is missing in the data. The third $\frac{5}{2}^+$ state in ^{17}F has not been known yet. We propose a known level at 8.43 MeV to be the $\frac{5}{2}^+$ state in ^{17}F based on its strength and angular distribution. Obtained S factors for the $\frac{5}{2}^+$ states of ^{17}O and ^{17}F are

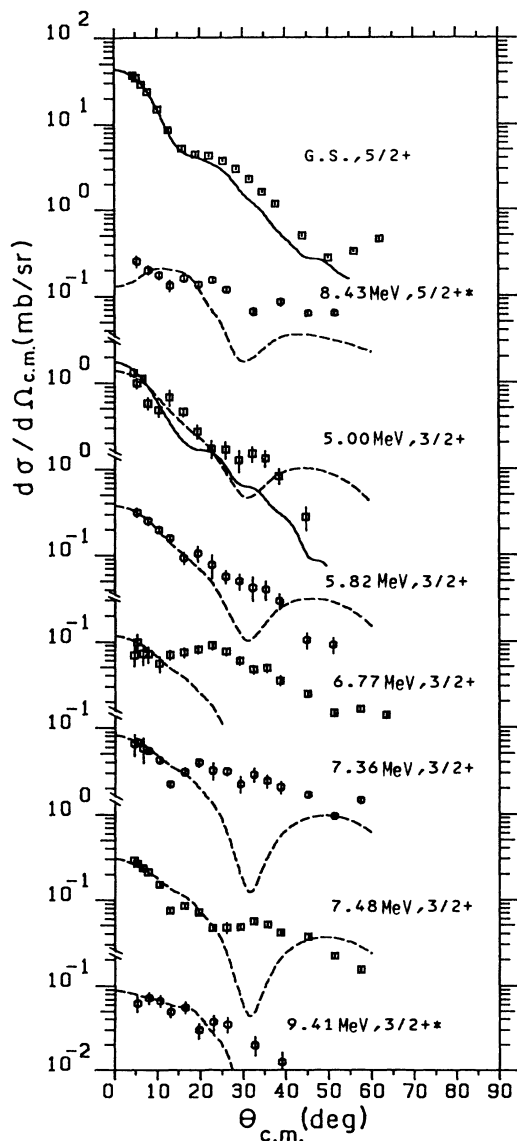


FIG. 5. Cross sections for the $^{16}\text{O}(\alpha, t)$ reaction leading to the $\frac{5}{2}^+$ and $\frac{3}{2}^+$ states in ^{17}F . See text and caption for Fig. 4.

about 0.15. Thus most $d_{5/2}$ strength is concentrated in the ground states in agreement with the shell model.

All the known $\frac{3}{2}^+$ states in ^{17}O and ^{17}F are unbound. Their angular distributions are compared with the ZR DWBA calculations with resonance form factors in Figs. 4 and 5. An EFR DWBA calculation with a loosely bound form factor is also shown for the 5.00 MeV $\frac{3}{2}^+$ state in ^{17}F . The 6.97 MeV state in ^{17}O and a new level at 9.41 MeV in ^{17}F are proposed to be $\frac{3}{2}^+$, corresponding to the 6.77 MeV $\frac{3}{2}^+$ state of ^{17}F and to the 9.78 MeV $\frac{3}{2}^+$ state of ^{17}O , respectively, based on the similarity of the excitation energies, strengths, and angular distributions, although the fits to the DWBA shapes are poor.

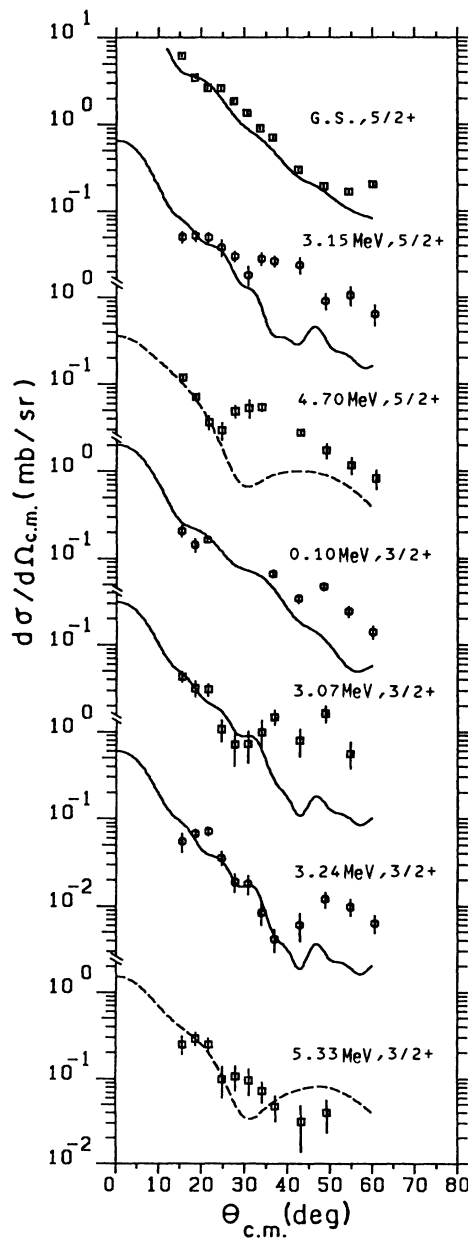


FIG. 6. Cross sections for the $^{18}\text{O}(\alpha, ^3\text{He})$ reaction leading to the $\frac{5}{2}^+$ and $\frac{3}{2}^+$ states in ^{19}O . See caption for Fig. 4.

The summed spectroscopic factors for the $0d_{3/2}$ transfer are 0.97 and 0.91 in ^{17}O and ^{17}F , respectively. The third $\frac{3}{2}^+$ state is not included in the sum because of the nonstripping pattern of the angular distribution. The strengths for the $0d_{3/2}$ transfer are distributed between 5 and 9 MeV in ^{17}O and ^{17}F , showing a clear difference from a simple shell model picture.

B. $(\alpha, ^3\text{He})$ and (α, t) reactions on ^{18}O with $l=2$ transfer

Figures 6 and 7 show the cross sections for the $\frac{5}{2}^+$ and $\frac{3}{2}^+$ states in ^{19}O and ^{19}F , respectively. Obtained strength distributions are in good agreement with the shell-model

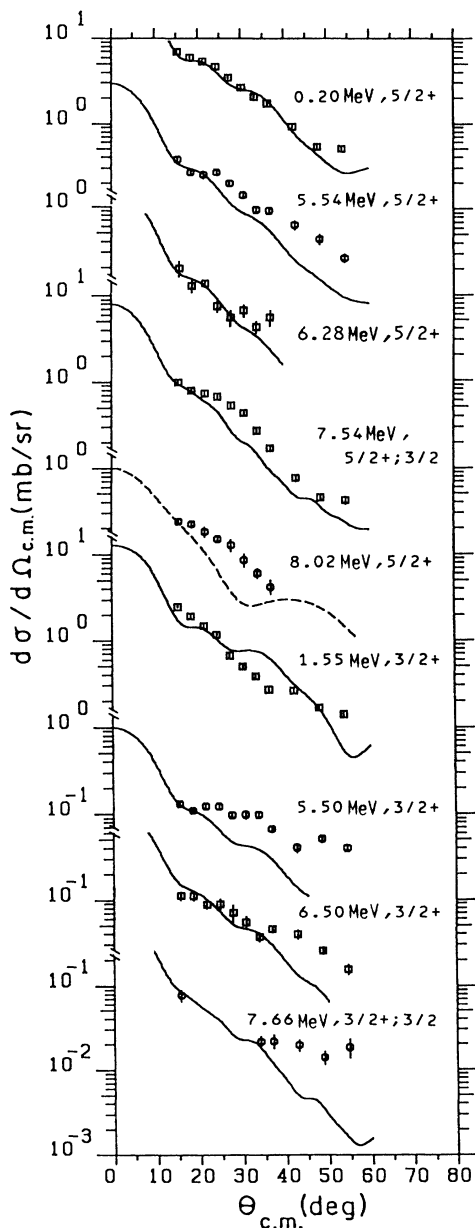


FIG. 7. Cross sections for the $^{18}\text{O}(\alpha, t)$ reaction leading to the $\frac{5}{2}^+$ and $\frac{3}{2}^+$ states in ^{19}F . See caption for Fig. 4.

predictions. The summed C^2S values for the $d_{5/2}$ transfer are 1.0 and 1.08 for ^{19}O and ^{19}F , respectively and 30% larger than the theoretical values [1] (see Table II).

The strongest $d_{3/2}$ transitions show different behaviors between the $T=\frac{1}{2}$ and $T=\frac{3}{2}$ states. The spectroscopic factor for the $T=\frac{1}{2}, \frac{3}{2}^+$ state at 1.55 MeV in ^{19}F is two times as large as the shell-model value, while that for the $T=\frac{3}{2}, \frac{3}{2}^+$ state at 5.33 MeV in ^{19}O is only a half of the prediction. The $d_{3/2}$ strengths reported in previous papers [18,19] for ^{19}O and ^{19}F are consistent with the shell model. In these papers, however, the data were taken at lower incident energies, and loosely bound form factors were used in the analyses for the unbound states resulting in larger spectroscopic factors. They also reported the

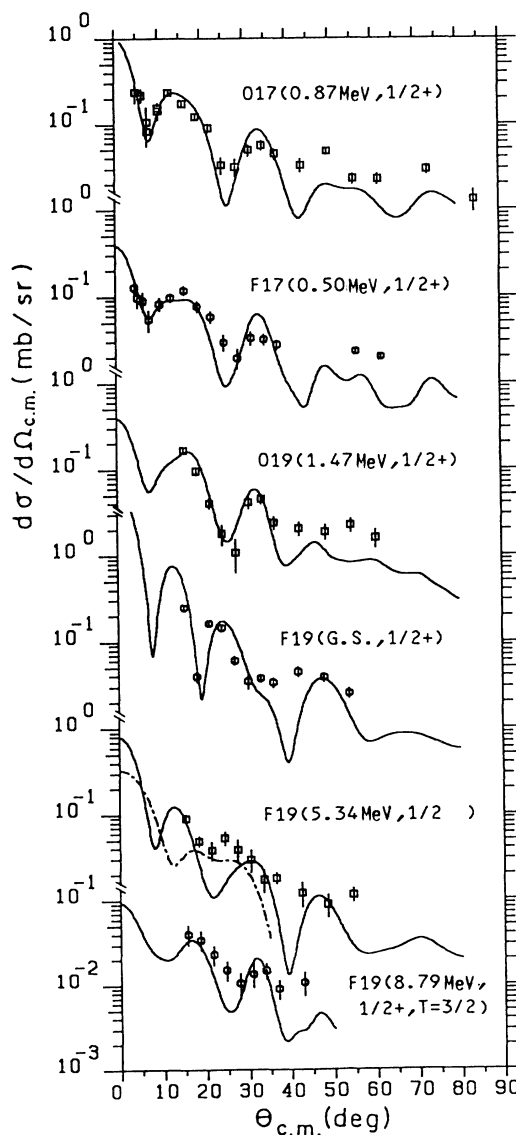


FIG. 8. Cross sections for the $(\alpha, ^3\text{He})$ and (α, t) reactions on ^{16}O and ^{18}O leading to the $\frac{1}{2}^+$ states. The solid curves are EFR DWBA calculations for the $1s_{1/2}$ transfer. The dot-dashed curve is for the $1p_{1/2}$ transfer. See caption for Fig. 4.

spectroscopic factors for the $T = \frac{3}{2}, \frac{5}{2}^+$ states in ^{19}O and ^{19}F differing by a factor of 1.7. In the present analysis, almost equal C^2S values are obtained for this analog pair.

Shell-model calculations [1] predict that most of the $\frac{3}{2}^+$ strength in ^{19}O is concentrated in the third $\frac{3}{2}^+$ state and very small fractions are distributed among the 0.29, 3.75, and 8.21 MeV states. More strengths are found experimentally in low-lying states with an additional $\frac{3}{2}^+$ state at 3.07 MeV. The spectroscopic factor for the lowest $T = \frac{3}{2}, \frac{3}{2}^+$ state in ^{19}F is considerably larger than the shell-model value.

C. $\frac{1}{2}^+$ states in $A = 17$ and 19 nuclei

Figure 8 shows the $(\alpha, ^3\text{He})$ and (α, t) angular distributions leading to the $\frac{1}{2}^+$ states in ^{17}O , ^{17}F , ^{19}O , and ^{19}F . Those for low-lying states are very well reproduced by the EFR DWBA calculations. Only one $\frac{1}{2}^+$ state was observed in each of ^{17}O , ^{17}F , and ^{19}O , and its spectroscopic factor is consistent with the shell-model prediction.

A small but well-isolated peak corresponding to the 8.79 MeV $\frac{1}{2}^+, T = \frac{3}{2}$ state in ^{19}F is seen in Fig. 2(b). The angular distribution for this state, which is unbound by 0.8 MeV, is less diffractive than that for the bound analog in ^{19}O , and agrees with the $l = 0$ DWBA curve. The 5.34 MeV state in ^{19}F has been assigned [7] as $J = \frac{1}{2}$. The measured angular distribution for this state is compared with calculated $l = 0$ (solid) and $l = 1$ (dot-dashed) curves in Fig. 8. The present data cannot give an unambiguous l assignment.

There are three known $\frac{1}{2}^+, T = \frac{1}{2}$ states in ^{19}F at 5.94, 6.26, and 7.36 MeV. Their cross sections for the (α, t) reaction are displayed in Fig. 9. These states are excited

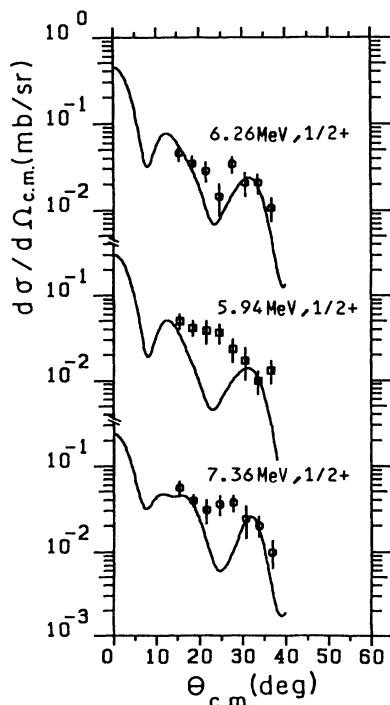


FIG. 9. Cross sections for the $^{18}\text{O}(\alpha, t)$ reaction leading to the $\frac{1}{2}^+$ states in ^{19}F . See caption to Fig. 4.

very weakly in the (α, t) reaction, and do not appear as clear peaks in Fig. 2(b). The 6.26 MeV state is located close to the 6.28 MeV $\frac{5}{2}^+$ state, and the cross sections for these states were obtained from peak fitting with fixed peak positions. The angular distribution for the 6.26 MeV $\frac{1}{2}^+$ state is reproduced by the DWBA calculation, and the deduced spectroscopic factor is in good agreement with the calculated value for the third $\frac{1}{2}^+, T = \frac{1}{2}$ state. Those for the 5.94 and 7.36 MeV states are less diffractive and different from the DWBA curves, probably due to multistep processes via inelastic channels. The spectroscopic factors for these states are an order of magnitude larger than the shell-model values if we identify them as the second and the fourth $\frac{1}{2}^+, T = \frac{1}{2}$ states.

The summed C^2S values for the $\frac{1}{2}^+$ states in ^{19}F is 1.05, if the 5.94 and 7.36 MeV are not included because of their nonstripping characters, in good agreement with the theoretical value of 0.96.

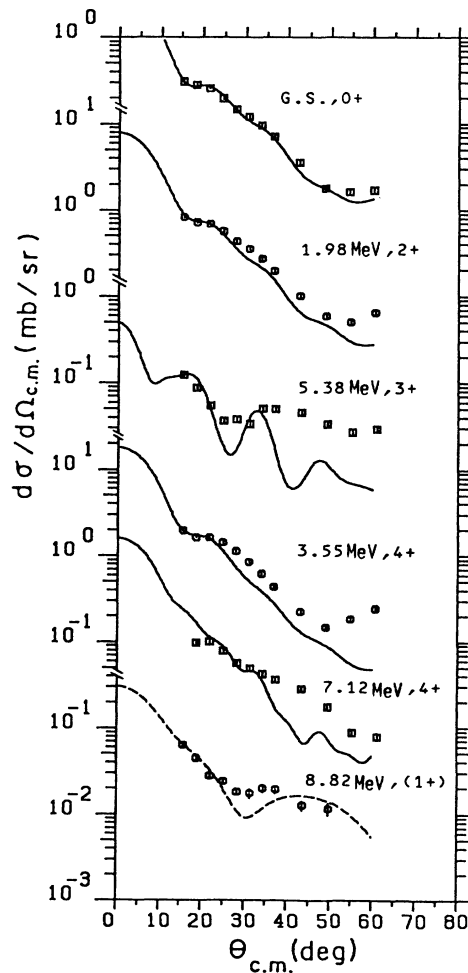


FIG. 10. Cross sections for the $^{17}\text{O}(\alpha, ^3\text{He})$ reaction leading to the positive-parity states in ^{18}O . The curves are EFR (solid) and ZR (dashed) DWBA calculations using the shell-model spectroscopic factors in Table III.

D. Positive-parity states in ^{18}O and ^{18}F

The cross sections for $(\alpha, ^3\text{He})$ and (α, t) reactions leading to positive-parity states in ^{18}O and ^{18}F are displayed in Figs. 10 and 11, respectively. The angular distributions for most of the states are well reproduced by the calculated curves at forward angles. The shell model also gives good accounts of the (α, t) strengths for most of the positive parity states in ^{18}F as shown in Table III and in Fig. 11. Exceptions are the 2_1^+ state at 2.52 MeV in ^{18}F , and the 4_2^+ state at 7.12 MeV and the 1_1^+ state at 8.82 MeV in ^{18}O , for which measured cross sections are much smaller than those predicted (Table III).

Larger $d_{3/2}$ and smaller $1s_{1/2}$ components than the shell model prediction are required for the 2.52 MeV 2_1^+ , $T=0$ state of ^{18}F to explain the angular distribution and

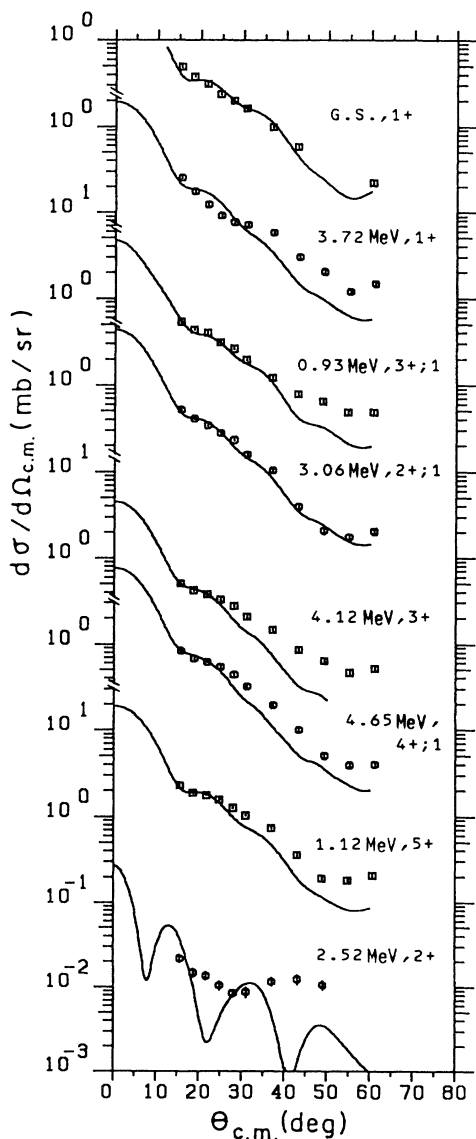


FIG. 11. Cross sections for the $^{17}\text{O}(\alpha, t)$ reaction leading to the positive-parity states in ^{18}F . See caption for Fig. 10.

the strength. The shell model predicts both the 4_2^+ and 1_1^+ states in ^{18}O to be excited mainly by the $d_{3/2}$ transfer. Hence the discrepancy between the experimental and calculated cross sections for these states suggests a poor description of the $0d_{3/2}$ single particle component in the shell model wave functions for ^{18}O . The theory also poorly describes the excitation energies. The calculated excitation energies for the 4_2^+ and 1_1^+ states are 1.63 MeV lower and 2.0 MeV higher, respectively, than the experimental energies, while most of the other states in ^{18}O are predicted within a few hundred keV of the experimental values.

Compared with the $T=1, 1^+$ state in ^{18}O , the (α, t) cross sections for the $T=0, 1^+$ states in ^{18}F at 0 MeV and 3.72 MeV show better agreement with the theory.

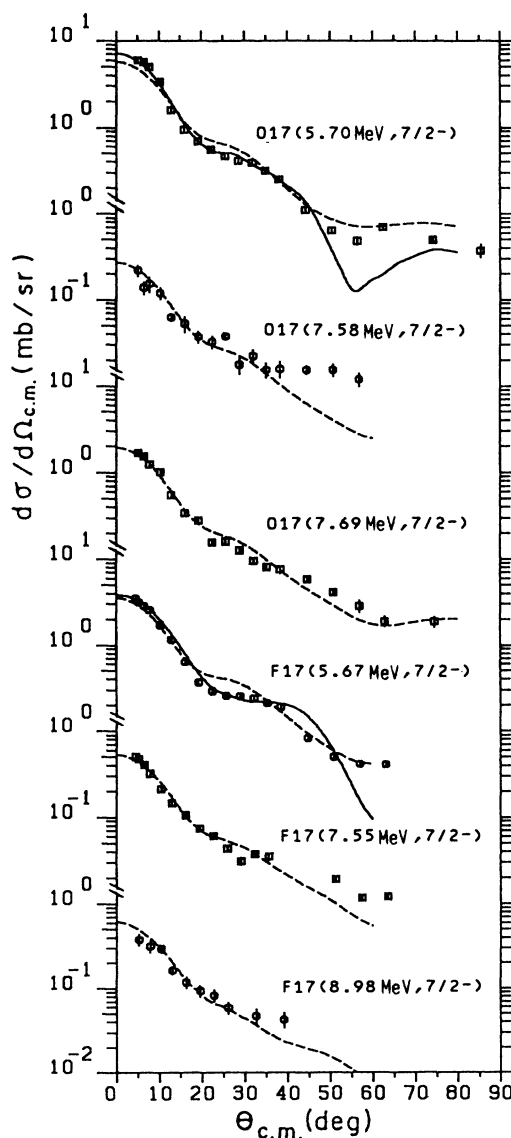


FIG. 12. Cross sections for the $(\alpha, ^3\text{He})$ and (α, t) reactions on ^{16}O leading to the $\frac{7}{2}^-$ states in ^{17}O and ^{17}F . The curves are EFR (solid) and ZR (dashed) DWBA calculations.

The main components of these transitions are $d_{5/2}$ as seen in Table III. However the ratio $\sigma_{\text{expt}}/\sigma_{\text{calc}}$ for the 1^+ ground state of ^{18}F is slightly larger than unity. The results for the 1_1^+ , $T=0$, state in ^{18}F and the 1_1^+ , $T=1$ state in ^{18}O seem to suggest that the former requires more, and the latter requires less, $d_{3/2}$ strength than the shell model predicts.

E. $\frac{7}{2}^-$ states in $A=17$ and 19 nuclei

Cross sections for the $(\alpha, ^3\text{He})$ and (α, t) reactions leading to the $\frac{7}{2}^-$ states of ^{17}O and ^{17}F are shown in Fig. 12, and those of ^{19}O and ^{19}F in Fig. 13. The solid (dashed) curves in these figures are EFR (ZR) DWBA calculations for the $0f_{7/2}$ transfer to the bound (unbound) states. In order to illustrate the difference between the EFR and

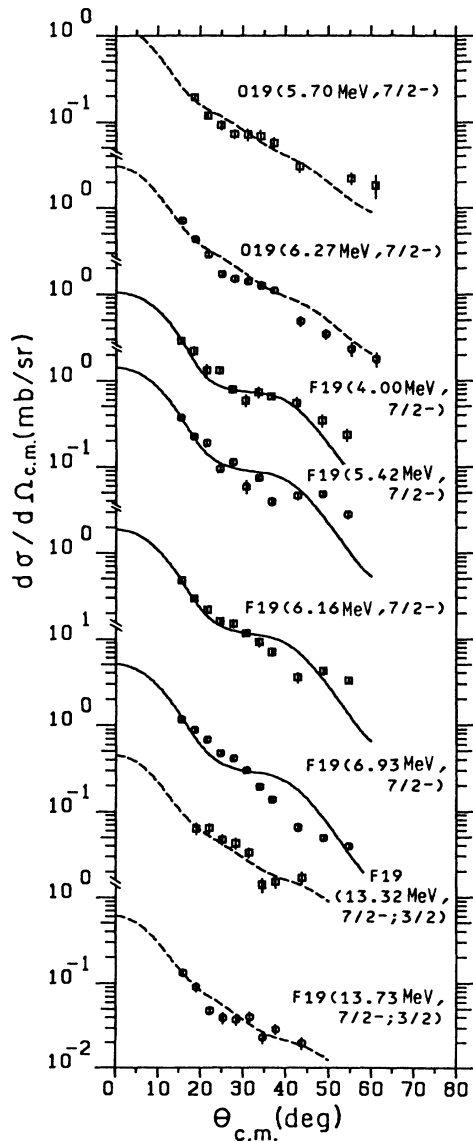


FIG. 13. Cross sections for the $(\alpha, ^3\text{He})$ and (α, t) reactions on ^{18}O leading to the $\frac{7}{2}^-$ states on ^{19}O and ^{19}F . See caption for Fig. 12.

ZR DWBA calculations, both are shown for the $\frac{7}{2}^-$ states in ^{17}O and ^{17}F which are unbound by 1.55 and 5.07 MeV, respectively. Both calculations give similar angular distribution shapes and similar spectroscopic factors for the $\frac{7}{2}^-$ state in ^{17}O . The difference between EFR and ZR calculations is larger for the $\frac{7}{2}^-$ state in ^{17}F which is more unbound. The spectroscopic factors for this analog pair are reasonably close to each other. It is notable that ZR DWBA calculations with resonance form factors give similar spectroscopic factors for the analog pair at 6.27 MeV in ^{19}O and 13.73 MeV in ^{19}F despite a large difference in the binding energies.

Another $\frac{7}{2}^-$, $T=\frac{3}{2}$ state is known [5] at 13.32 MeV in ^{19}F . The analog of this state is excited around 5.78 MeV in ^{19}O . As seen in Fig. 2(a), a peak was observed at $E_x = 5.70$ MeV in the $^{18}\text{O}(\alpha, ^3\text{He})^{19}\text{O}$ reaction. Its angular distribution is well described by an $f_{7/2}$ transfer (Fig. 13). Furthermore, the 5.70 MeV state has a spectroscopic factor almost the same as that for the 13.32 MeV $\frac{7}{2}^-$ state in ^{19}F . Thus the present results confirm a previous assignment of $J^x = \frac{7}{2}^-$ to the 5.70 MeV in the ^{19}O state based on polarization measurements [18] in the $^{18}\text{O}(d, p)^{19}\text{O}$ reaction, and suggest this state to be the

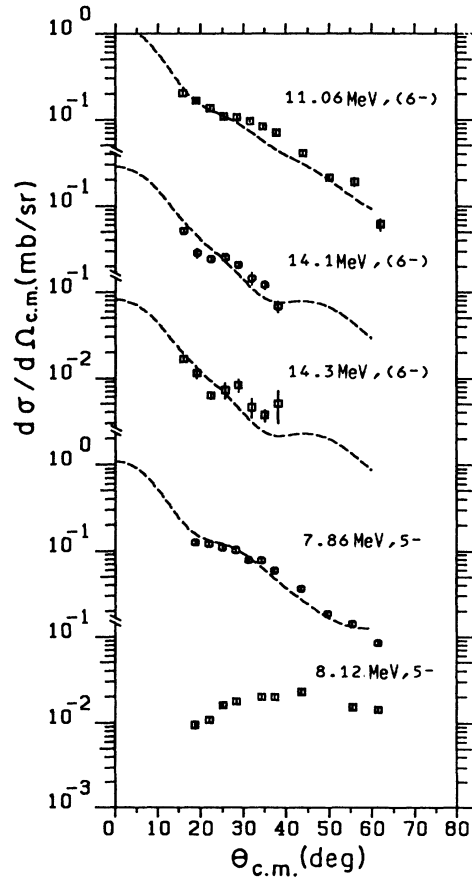


FIG. 14. Cross sections for the $^{17}\text{O}(\alpha, ^3\text{He})$ reaction leading to the 5^- and possible 6^- states in ^{18}O . The curves are ZR DWBA calculations for the $0f_{7/2}$ transfer.

analog of the 13.32 MeV state in ^{19}F .

The lowest $\frac{7}{2}^-$ state has the largest strength in ^{17}O and ^{17}F , while the second $\frac{7}{2}^-$ state is the stronger of the two $T=\frac{3}{2}$ states in ^{19}O and ^{19}F . A more complicated distribution of the strength is seen for the $\frac{7}{2}^-$, $T=\frac{1}{2}$ states in ^{19}F . The known lowest four $\frac{7}{2}^-$, $T=\frac{1}{2}$ states in ^{19}F at 4.00, 5.42, 6.16, and 6.93 MeV are populated with small S factors. These $\frac{7}{2}^-$ states are known [5, 22–24] to have a γ -decay branch to the core-polarized $\frac{5}{2}^-$ state at 1.35 MeV in addition to the decay to the $\frac{5}{2}^+$ single-particle state at 0.20 MeV. These results, combined with the present data, indicate that these states are primarily core-coupled states with a small fraction of single-particle component. The summed $f_{7/2}$ spectroscopic factor for ^{19}F is 0.14, nearly the same as that for ^{19}O , but smaller than those for ^{17}O and ^{17}F .

F. 6^- and 5^- states in ^{18}O and ^{18}F

A $0f_{7/2}$ nucleon transfer on $^{17}\text{O}(\text{g.s.}, \frac{5}{2}^+)$ can excite states with J^π from 1^- to 6^- . The 6^- and 5^- states are

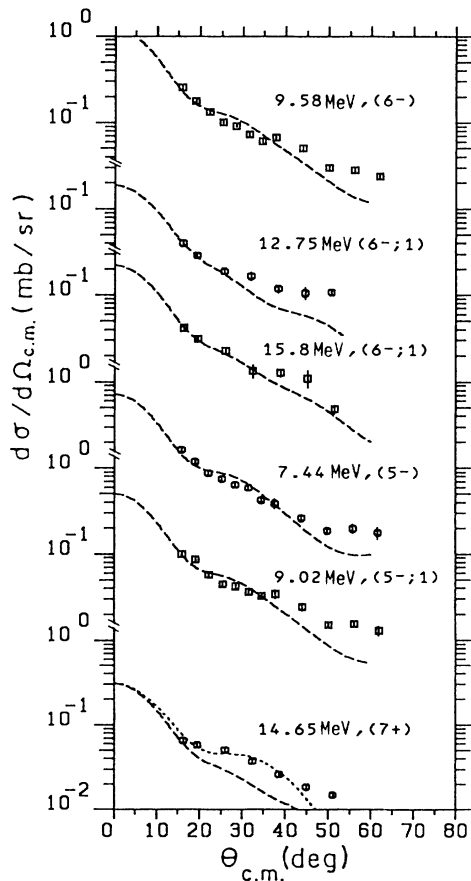


FIG. 15. Cross sections for the $^{17}\text{O}(\alpha, t)$ reaction with an angular momentum transfer $l=3$ or 4. See text and caption for Fig. 14.

excited by pure $l=3$, while $l=1$ mixtures are possible for states with $J^\pi=1^-$ to 4^- . In this section we discuss only the states which show pure $l=3$ angular distributions in the $^{17}\text{O}(\alpha, ^3\text{He})^{18}\text{O}$ and $^{17}\text{O}(\alpha, t)^{18}\text{F}$ reactions shown in Figs. 14 and 15.

There are two well-established 5^- states in ^{18}O , one at 7.86 MeV and the other at 8.12 MeV [5]. The 7.86 MeV state indeed shows a characteristic $l=3$ angular distribution. On the other hand, the cross section for the 8.12 MeV state is an order of magnitude smaller with a flat angular distribution, suggesting very small single-particle component in this state.

The 14.1 and 14.3 MeV states in ^{18}O were proposed to be 6^- in an (e, e') experiment [7]. The observed $l=3$ ($\alpha, ^3\text{He}$) angular distributions to these states (Fig. 14) are consistent with the 6^- assignments. Then the analog of these states in ^{18}F are expected around 15 MeV. The (α, t) angular distribution for the 15.8 MeV state of ^{18}F shows an $l=3$ pattern, and is tentatively assigned as 6^- , $T=1$. No evidence for another nearby 6^- state was found. The 14.65 MeV state of ^{18}F , whose cross sections are comparable to those for the 15.8 MeV state, seems to show an $l=4$ angular distribution rather than $l=3$ (Fig. 15).

A 6^- , $T=0$ state of ^{18}F is expected around 8–9 MeV. Three states at 9.58, 9.02, and 7.44 MeV have angular distributions characteristic of $l=3$. The 9.02 MeV state seems to be the analog to the 7.86 MeV 5^- state of ^{18}O from its energy and the spectroscopic factor. The 7.44 MeV state was not observed in the $^{16}\text{O}(\alpha, d)^{18}\text{F}$ reaction [10]. The (α, d) cross section for a 5^- state with the $(d_{5/2}f_{7/2})$ configuration is suppressed by two orders of magnitude or more compared with that for the stretched 6^- state because of the $9j$ symbol. Thus the strong excitation of the 7.44 MeV state in the $(\alpha, ^3\text{He})$ reaction together with the (α, d) result makes a 5^- assignment very likely to this state. It has an isospin $T=0$, since no corresponding state was observed in ^{18}O with comparable strength. These arguments leave the 9.58 MeV state as the only candidate for the 6^- , $T=0$ state. This state has been assigned [6] as 6^+ , which would require $l=4$ in single proton in single proton transfers. On the other hand, a 6^- assignment was given in a study of [10] of the $^{16}\text{O}(\alpha, d)^{18}\text{F}$ reaction based on the angular distribution shape and the cross section strength. (The energy of this state was mistakenly labeled 9.49 MeV in Ref. [10].) The present data prefer J^π of 6^- for the 9.58 MeV state of ^{18}O in agreement with the (α, d) result.

The 11.06 MeV state in ^{18}O and the 12.75 MeV state in ^{18}F seem to be an analog pair from their energies, cross section strengths, and angular distributions. We tentatively give 6^- , $T=1$ assignment to these states since the lowest 6^- , $T=1$ states would be expected in this region, about 2–3 MeV above the 6^- , $T=0$ state. Although we could not exclude a possibility of $l=4$, from their angular distributions, it is unlikely that states with a considerable $l=4$ strength appear so low in energy.

The states discussed above are listed in Table IV with the deduced spectroscopic factors. The summed C^2s values in ^{18}O and ^{18}F are similar and about 10–15% of the sum-rule limit.

TABLE II. Spectroscopic factors for the $(\alpha, {}^3\text{He})$ and (α, t) reactions on ${}^{16}\text{O}$ and ${}^{18}\text{O}$. The E_x and J^π values are cited from Ref. [5]. Those with a dollar sign are proposed in the present work. Spectroscopic factors with an asterisk are obtained from EFR DWBA calculations. Those without are from ZR DWBA calculations. The summed spectroscopic strength $\sum C^2S$ for each NLJ transfer is given in angular brackets. A double asterisk means EFR calculations with potential parameter sets A1-HB in Table I.

Nuclei	Final states E_x (MeV)	J^π	σ_{INT} (mb)	$NL2J$	Spectroscopic factors		Calc. ^a
					Present	Expt. Previous	
${}^{17}\text{O}$	g.s.	$\frac{5}{2}^+$	12.1	$0D5$	1.3* (1.0**)	$\sim 0.9^b$	1
	8.40	$\frac{5}{2}^+$	0.29	$0D5$	0.15 $\langle 1.5 \rangle$		$\langle 1 \rangle$
	0.87	$\frac{1}{2}^+$	0.23	$1S1$	0.90* $\langle 0.90 \rangle$	$\sim 0.9^b$	1 $\langle 1 \rangle$
	5.09	$\frac{3}{2}^+$	0.77	$0D3$	0.67	1.2 ^c	1
	5.87	$\frac{3}{2}^+$	0.08		0.06		
	6.97	$\frac{3}{2}^+$	0.15		(0.08)		
	9.78	$\frac{3}{2}^+$	0.15		0.24 $\langle 0.97 \rangle$		$\langle 1 \rangle$
	5.70	$\frac{7}{2}^-$	1.42	$0F7$	0.17 (0.18*)	0.15 ^c	
	7.58	$\frac{7}{2}^-$	0.07		0.01		
	7.69	$\frac{7}{2}^-$	0.45		0.10 $\langle 0.30 \rangle$		
	7.75	$\frac{11}{2}^-$	0.62				
	${}^{17}\text{F}$	g.s.	$\frac{5}{2}^+$	7.2	$0D5$	1.3* (1.0**)	0.93 ^d
8.43		$\frac{5}{2}^+$ ^{\\$}	0.22		0.13 $\langle 1.4 \rangle$		$\langle 1 \rangle$
0.50		$\frac{1}{2}^+$	0.11	$1S1$	0.75* $\langle 0.75 \rangle$	0.84 ^d	1 $\langle 1 \rangle$
5.00		$\frac{3}{2}^+$	0.36	$0D3$	0.54 (0.55*)		1
5.82		$\frac{3}{2}^+$	0.12		0.17		
6.77		$\frac{3}{2}^+$	0.13		(0.06)		
7.36		$\frac{3}{2}^+$	0.06		0.03		
7.48		$\frac{3}{2}^+$	0.14		0.13		
9.41		$(\frac{3}{2}^+)^{\$}$	0.04		0.04 $\langle 0.91 \rangle$		$\langle 1 \rangle$
5.67		$\frac{7}{2}^-$	0.82	$0F7$	0.14 (0.21*)		
7.55		$\frac{7}{2}^-$	0.14		0.03		
8.92		$\frac{7}{2}^-$	0.12		0.06 $\langle 0.23 \rangle$		
${}^{19}\text{O}$	g.s.	$\frac{5}{2}^+$	2.60	$0D5$	0.90*	0.57 ^e	0.685
	3.15	$\frac{5}{2}^+$	0.06		0.03		0.021

TABLE II. (Continued).

Nuclei	Final states E_x (MeV)	J^π	σ_{INT} (mb)	$NL2J$	Spectroscopic factors		Calc. ^a
					Present	Expt. Previous	
	4.70	$\frac{5}{2}^+$	0.09		0.07		0.006
					$\langle 1.0 \rangle$		$\langle 0.71 \rangle$
	1.47	$\frac{1}{2}^+$	0.08	1S1	0.86*	1.0 ^e	0.83
					$\langle 0.86 \rangle$		$\langle 0.83 \rangle$
	0.10	$\frac{3}{2}^+$	0.19	0D3	0.09*		0.013
	3.07	$\frac{3}{2}^+$	0.03		0.03*		–
	3.24	$\frac{3}{2}^+$	0.05		0.05*		0.009
	5.33	$\frac{3}{2}^+$	0.18		0.43	0.85 ^c	0.920
					$\langle 0.60 \rangle$		$\langle 0.94 \rangle$
	5.70	$\frac{7}{2}^-$ ^s	0.14	0F7	0.05		
	6.27	$\frac{7}{2}^-$	0.31		0.13		
					$\langle 0.18 \rangle$		
¹⁹ F	0.20	$\frac{5}{2}^+$	4.84	0D5	1.0*	0.51 ^f	0.730
					(0.97)		
	5.53	$\frac{5}{2}^+$	0.27		0.11*		0.121
	6.28	$\frac{5}{2}^+$	0.09		0.07*		0.042
	7.54	$\frac{5}{2}^+, T = \frac{3}{2}$	0.64		0.88*	0.33 ^f	0.685
	8.02	$\frac{5}{2}^+$	0.13		(0.1)		0.078
					$\langle 1.08 \rangle$		$\langle 0.88 \rangle$
	g.s.	$\frac{1}{2}^+$	0.13	1S1	0.38*	0.32 ^f	0.577
	5.34	$\frac{1}{2}^{(+)}\text{s}$	0.05	1S1	0.3*		–
				(1P1)	(0.01*)		
	5.94	$\frac{1}{2}^+$	0.03	1S1	(0.2)		0.014
	6.26	$\frac{1}{2}^+$	0.03		0.45		0.420
	7.36	$\frac{1}{2}^+$	0.03		(0.5)		0.016
	8.79	$\frac{1}{2}^+, T = \frac{3}{2}$	0.02		0.9		0.831
					(1.0*)		
					$\langle 1.05 \rangle$		$\langle 0.96 \rangle$
	1.55	$\frac{3}{2}^+$	1.22	0D3	0.62*	0.38 ^f	0.303
	5.5	$\frac{3}{2}^+$	0.17		0.07*		0.054
	6.5	$\frac{3}{2}^+$	0.11		0.09*	0.05 ^f	0.013
	7.66	$\frac{3}{2}^+, T = \frac{3}{2}$	0.09		0.13*	0.03 ^f	0.013
					$\langle 0.56 \rangle$		$\langle 0.38 \rangle$
	4.00	$\frac{7}{2}^-$	0.20	0F7	0.02*		
	5.42	$\frac{7}{2}^-$	0.18	0F7	0.02*		
	6.16	$\frac{7}{2}^-$	0.23		0.03*		
	6.93	$\frac{7}{2}^-$	0.56		0.07*		
	13.32	$\frac{7}{2}^-, T = \frac{3}{2}$ ^s	0.04		0.04		
	13.73	$\frac{7}{2}^-, T = \frac{3}{2}$	0.06		0.11		
					$\langle 0.14 \rangle$		

^aShell-model calculations with the code INS [21] using the Wildenthal interaction [1].

^bReference [15].

^cReference [16].

^dReference [17].

^eReference [18].

^fReference [19].

TABLE III. Spectroscopic information for the $^{17}\text{O}(\alpha, ^3\text{He})$ and (α, t) reactions leading to the positive-parity states in ^{18}O and ^{18}F .

Nuclei	Final states ^a E_x (MeV)	J^π	σ_{INT} (mb)	Calculated spectroscopic factor ^b			$\sigma_{\text{expt}}/\sigma_{\text{calc}}$	
				$D5$	$1S1$	$D3$	Present ^d	Previous ^c
^{18}O	g.s.	0^+	0.22	1.58			0.86 (0.82*)	0.77
	1.98	2^+	0.64	1.21	0.33	0.01	0.79	
	3.55	4^+	1.59	1.87		0.07	0.84	0.82
	5.38	3^+	0.12		0.98	0.02	1.04	1.01
	7.12	4^+	0.09	0.13		0.93	0.31	
	8.82	(1^+)	0.04			0.85	0.55*	
^{18}F	g.s.	1^+	0.26	0.57		0.38	1.38	
	0.93	3_1^+	0.41	0.64	0.63	0.05	0.78	
	1.04	$0^+, T=1$		1.58				
	1.12	5^+	1.92	2			1.04 (1.02*)	
	2.52	2^+	0.02		0.89	0	0.36	
	3.06	$2^+, T=1$	0.32	1.21	0.33	0.01	1.11	
	3.72	1^+	0.15	1.06		0.003	1.04	
	4.11	3_3^+	0.43	1.22 ^c	0.36 ^c	0.02 ^c	0.96	
	4.65	$4^+, T=1$	0.61	1.87		0.07	0.94	

^aReference [5].^bReferences [1] and [21].^cValues of S_{calc} for the second 3^+ state.^dDeduced from the EFR DWBA calculations. Those with an asterisk are from the ZR DWBA calculations.^eReference [20].

V. SUMMARY

Cross sections for the $(\alpha, ^3\text{He})$ and (α, t) reactions in oxygen isotopes were measured over a wide range of excitation energies. Many spin-parity and isospin assignments were proposed from comparisons of the strengths, angular distributions, and excitation energies.

The exact-finite-range DWBA analyses of these reactions leading to bound states reproduced the angular distribution shapes for the $0d_{5/2}$ and $1s_{1/2}$ transfers. Nearly full $0d_{5/2}$, $1s_{1/2}$, and $0d_{3/2}$ strengths were observed in the present measurement. Almost identical strengths were obtained for all the analog pairs in spite of an about 4

TABLE IV. Spectroscopic factors for the 6^- and 5^- states in ^{18}O and ^{18}F . Values in brackets are summed spectroscopic factors.

Nuclei	Final states		σ_{INT} (mb)	$NL2J$	Spectroscopic factor
	E_x (MeV)	J^π			
^{18}O	11.06	$(6^-)^a$	0.18	$0F7$	0.27
	14.1	$(6^-)^b$	0.02		0.16
	14.3	$(6^-)^b$	0.01		0.05
					(0.48)
	7.86	5^-^c	0.14	$0F7$	0.09
	8.12	5^-^c	0.06	$(0F7)$	
^{18}F	9.58	$(6^-)^a$	0.19	$0F7$	0.29
	12.75	$(6^-, T=1)$	0.03		0.12
	15.8	$(6^-, T=1)^a$	0.03		0.02
					(0.31)
	7.44	$(5^-)^a$	0.09	$0F7$	0.13
	9.02	$(5^-, T=1)^a$	0.09		0.13
					(0.13)
	14.65	$(7^+)^a$	0.07	$0G9$	0.10

^aA J^π value assumed in the present analysis.^bReference [7].^cReference [5].

MeV difference in the binding energies, except for the 2_1^+ , $T=1$ states on ^{18}O and ^{18}F . DWBA calculations with resonance form factors were required for unbound states to give similar spectroscopic factors for the analog pairs.

The present data and analysis have led to a detailed comparison of the spectroscopic factors with the shell-model calculations by Wildenthal. An excellent agreement between the experiment and the theory was found for the $0d_{5/2}$ and $1s_{1/2}$ strength distributions, while considerable deviations from the theory were observed for the $0d_{3/2}$ transfers. The $d_{3/2}$ strengths are more fragmented in ^{17}O and ^{17}F than the shell-model calculations. The energy gap between the centroids of the $d_{5/2}$ and $d_{3/2}$ shell orbits is 5.43 MeV in ^{17}O and 5.05 MeV in ^{17}F , somewhat smaller than 5.59 MeV assumed in the shell-model calculation. The deduced spectroscopic factors for the $\frac{3}{2}^+$ states in $A=19$ nuclei were larger for the $T=\frac{1}{2}$ states, and smaller for the $T=\frac{3}{2}$ states, than the predicted

values. The ratio of the experimental to the calculated cross sections $\sigma_{\text{expt}}/\sigma_{\text{calc}}$ were almost unity for the positive-parity states in ^{18}O and ^{18}F with major $d_{5/2}$ and $1s_{1/2}$ components, while the ratios deviate from unity for states with a large $d_{3/2}$ component.

The summed strengths of the C^2S values for the 6^- states in ^{18}O and ^{18}F were consistent with those for the $\frac{7}{2}^-$ states in ^{17}O and ^{17}F . The observed $0f_{7/2}$ strength was 10–30 % of the sum-rule limit in all cases.

ACKNOWLEDGMENTS

We are grateful to Prof. T. Suzuki of the Research Center for Nuclear Physics, Osaka University, for valuable discussions. Numerical calculations were carried out with the central computers at the Research Center for Nuclear Physics, Osaka University, and at Kantogakuin University.

-
- [1] B. H. Wildenthal, *Prog. Part. Phys.* **11**, 5 (1984); Proceedings of Yamada Conference XXIII on Nuclear Weak Processes and Nuclear Structure, Osaka, 1989, edited by M. Morita *et al.* (World Scientific, Singapore, 1989), p. 314.
- [2] P. M. Endt, P. de Wit, C. Alderliesten, and B. H. Wildenthal, *Nucl. Phys.* **A487**, 221 (1988).
- [3] M. Yasue *et al.*, *Phys. Rev. C* **42**, 1279 (1990).
- [4] M.-F. Jiang, R. Machleidt, D. B. Stout, and T. T. S. Kuo, *Phys. Rev. C* **40**, 1857 (1989).
- [5] F. Ajzenberg-Selove, *Nucl. Phys.* **A460**, 70 (1986); *ibid.* **A475**, 1 (1987).
- [6] C. Djalali, G. M. Crawley, B. A. Brown, V. Rotberg, G. Caskey, and A. Galonsky, *Phys. Rev. C* **35**, 1201 (1987).
- [7] D. M. Manley *et al.*, *Bull. Am. Phys. Soc.* **35**, 927 (1990).
- [8] S. Kato, M. H. Tanaka, and T. Hasegawa, *Nucl. Instrum. Methods* **154**, 19 (1978).
- [9] M. H. Tanaka, S. Kubono, and S. Kato, *Nucl. Instrum. Methods* **195**, 509 (1982).
- [10] Y. Kadota, K. Ogino, T. Tanabe, and M. Yasue, *Nucl. Phys.* **A458**, 523 (1986).
- [11] M. Igarashi, One-step and two-step exact-finite-range DWBA code (unpublished).
- [12] P. D. Kunz, Zero-range DWBA code, University of Colorado (unpublished).
- [13] L. F. Hansen, J. L. Kammerdiener, and M. S. Weiss, *Phys. Rev.* **174**, 1155 (1968).
- [14] F. D. Becchetti and G. W. Greenlees, in *Polarization Phenomena in Nuclear Reactions*, edited by H. H. Barschall and W. Haeblerli (The University of Wisconsin Press, Madison, 1971), p. 682.
- [15] M. D. Cooper, W. F. Hornyak, and P. G. Roos, *Nucl. Phys.* **A218**, 249 (1974).
- [16] S. D. Darden, S. Sen, H. R. Hiddleston, J. A. Aymar, and W. A. Yoh, *Nucl. Phys.* **A208**, 77 (1973).
- [17] H. T. Fortune, L. R. Medsker, J. P. Garrett, and H. G. Bingham, *Phys. Rev. C* **12**, 1723 (1975).
- [18] S. Sen, S. E. Darden, H. R. Hiddleston, and W. A. Yoh, *Nucl. Phys.* **A219**, 429 (1974).
- [19] C. Schmidt and H. H. Duhm, *Nucl. Phys.* **A155**, 644 (1970).
- [20] T. K. Li, D. Dehnhard, R. E. Brown, and P. J. Ellis, *Phys. Rev. C* **13**, 55 (1976).
- [21] K. Ogawa, shell model calculation code (unpublished).
- [22] W. R. Dixon and R. S. Storey, *Nucl. Phys.* **A284**, 97 (1977).
- [23] D. W. O. Rogers, R. P. Beukens, and W. T. Diamond, *Can. J. Phys.* **50**, 2428 (1972).
- [24] K. Bharuth-Ram, K. P. Jackson, P. G. Lawson, N. A. Jelley, and K. W. Allen, *Nucl. Phys.* **A269**, 327 (1976).